Research Article | Vol. 27, No. 5 | 4 Mar 2019 | OPTICS EXPRESS 7560
Optics EXPRESS

Polyethersulfone optical fibers with thermally induced microbubbles for custom side-scattering profiles

SOROUSH SHABAHANG,[1] SARAH FORWARD,[1] AND SEOK-HYUN YUN[1,2,*]

[1]*Harvard Medical School and Wellman Center for Photomedicine, Massachusetts General Hospital, 50 Blossom Street, Boston, Massachusetts, USA, 02114*
[2]*Harvard-MIT Health Sciences and Technology, Massachusetts Institute of Technology, 77 Massachusetts Avenue, Cambridge, Massachusetts, USA, 02139*
[*]*syun@hms.harvard.edu*

Abstract: Polyethersulfone (PES) optical fibers are drawn and thermally processed in order to generate variable side-illumination profiles. The thermal treatment allows microbubbles to be formed in an outer layer of the PES fiber, providing light scattering with controllable amplitudes (0.25-2.5 cm^{-1}). Several fibers with different scattering profiles, such as uniform axial irradiation and multiple irradiation spots, are demonstrated. A small microbubble-induced scattering spot on the surface may be used for side-coupling of ambient light into the fiber. These mechanically flexible all-PES fibers with custom-designable scattering profiles may be useful for spatially tuned delivery of light for various applications, including phototherapy.

1. Introduction

Optical fibers and waveguides have been conventionally designed to emit light from their ends. In various medical applications that require fiber-optic light delivery, such as imaging, laser surgery and phototherapy in hollow organs, side illumination is often a preferred method [1]. This is achieved by having the fiber tip polished at 45 degrees or attached with a micro prism to direct the optical beam to the side. To cover a macroscopically large tissue area as typically required in photodynamic therapy (PDT), such a side-emitting fiber is inserted into the distal end of target tissue and slowly pulled out while it is rotated [2,3]. However, this scanning technique increases the procedure time and requires skilled operator expertise. More sophisticated, radially-diffusive optical fiber microneedles have been developed, eliminating the need for rotation [4,5], but still necessitate an axial scan for applications beyond superficial sites (>3 mm in depth). For scan-free side illumination, tapered fibers [6] and surface-patterned implantable waveguides [7] have been demonstrated. Nevertheless, it remains challenging to obtain a uniform emission profile over a large, desirable area emitted directly from an optical fiber [8,9]. While uniform illumination is desirable for tissue- or organ-scale therapies, the recent applications of light at the microstructural and cellular levels, such as optogenetics [10,11], require more complex, spatial illumination patterns at multiple discrete locations. For these applications, an array of end-firing optical fibers has been used [12]. In addition, implantable probes employing an assembly of micro light-emitting diodes have also been developed [10,13]. A user-designed side-emitting optical fiber may be an attractive alternative for such applications.

In this paper, we present novel, polymeric optical fibers and a simple thermal post-processing method to enable custom-patterned side illumination. We use poly(ethersulfone) (PES), a heat-resistant thermoplastic polymer [14] with a glass transition temperature of 220-250°C. PES shows low optical attenuation in the long visible and infrared wavelengths with a refractive index of 1.65, shown in Fig. 1(a). Due to its mechanical strength, PES has been used as the support material of outer jackets of otherwise fragile glass optical fibers [15–17].

#356475 https://doi.org/10.1364/OE.27.007560
Journal © 2019 Received 28 Dec 2018; revised 4 Feb 2019; accepted 8 Feb 2019; published 28 Feb 2019

Optics EXPRESS

Some other interesting mechanical properties of PES have been studied elsewhere [18]. A generally overlooked—but important in this work— property of PES is that it possesses a high water absorption capacity of ~2% at equilibrium [19–21]. This considerable water retention enables us to generate microbubbles, via thermal post-treatment, in customizable patterns for side scattering. The light-diffusing elements are formed inside the fiber, unlike most conventional modified fibers, which can add to stability against variation of surrounding tissues.

2. Experimental results

2.1 Drawing PES fibers from thermoplastic preforms

A homebuilt drawing furnace was used for thermal fiber drawing, consisting of a 10 cm-long cylindrical heater with an inner diameter of 10 cm. The temperature of the hottest section of the heater was approximately 250 °C. Before drawing, we placed a PES rod preform, shown in Fig. 1(b), in vacuum for 48 h at 100 °C to remove moisture from the polymer. This step is important to reduce optical scattering loss after thermal drawing of the preform into the fiber form. Figure 1(c) depicts how the PES preform was then manually pulled downward through the furnace. The fiber thickness was controlled by the fiber pulling speed and the furnace temperature. Figure 1(d) shows a spool of a PES fiber drawn to a diameter of ~300 µm. Figure 1(e) illustrates red light (633 nm) propagating through a 30 cm-long PES fiber and dispersed beyond the distal, cleaved end.

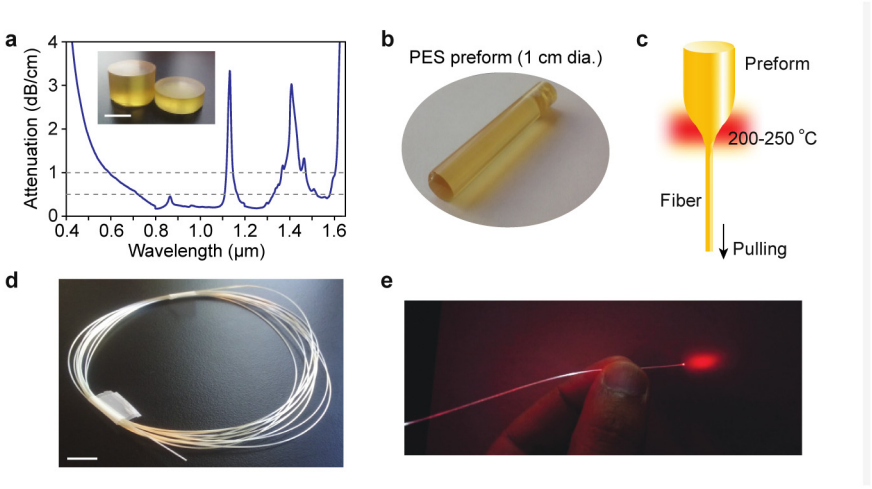

Fig. 1. (a) Measured spectral loss in dB/cm of PES bulk samples using a Bruker FTIR Spectrometer (inset scale bar = 1 cm). (b) Photograph of a 6-cm-long PES rod preform. (c) Illustration of the thermal drawing of the PES preform into fiber. (d) Photograph of a resulting PES fiber (scale bar = 1 cm). (e) A PES fiber delivering red light.

2.2 Formation of light-scattering structure by heat treatment

PES contains nano-sized pores in its polymeric network, as shown in Fig. 2. Moisture in the ambient air can easily penetrate and remain inside these pores. Heating PES creates an increased internal vapor pressure where moisture near the polymer surface escapes the material, but the moisture trapped farther inside the material expands and forms microbubbles, increasing the size of the polymer pores illustrated in Figs. 2(b) and 2(c). As the material is cooled below its softening temperature, the microbubble-enlarged pores are physically settled. At room temperature, the vapor pressure is equilibrated, but the micropores remain and serve as scattering elements. Rayleigh light scattering is dominant in the intact

Optics EXPRESS

polymer with nanopores, but after the heat treatment, Mie scattering becomes the dominant scattering, producing strong white-color scattering shown in Fig. 2(d).

Visual inspection under a brightfield microscope showed that microbubbles begin to appear in areas inside the polymer close to the surface, where the polymer's temperature is high, but the vapor has not escaped. The faster the temperature increases, the closer to the surface microbubbles were formed. The formation of bubbles near the surface serves as a thermal insulating layer and slows down the further heating of the inner polymer layers. Furthermore, the innermost bubbles may liberate vapor from the deepest layers. As a result, the inner region of the fiber remains intact. This low-scattering central part acts as a fiber core. Figure 2(e) shows the cross section of the fiber after heat treatment. More details on the microbubble distribution are described in Section 2.4.

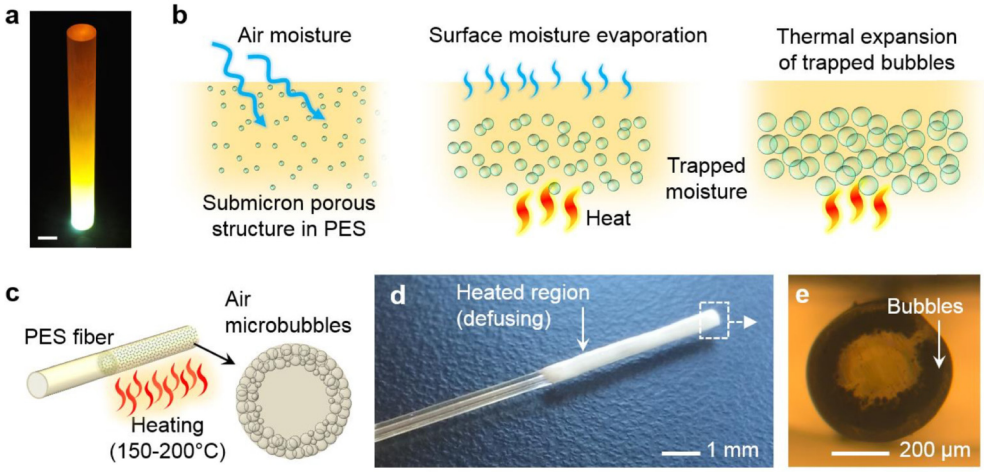

Fig. 2. (a) Rayleigh scattering from nanoscale pores shown in a 20 cm-long PES rod illuminated with white light from the bottom (scale bar = 1 cm). (b) Illustration showing the formation of diffusing air bubbles inside PES via external heating. (c) Illustration showing the conversion of a transparent PES fiber into a scattering fiber by the heat treatment. (d) Photograph of a PES fiber after heat treatment in the distant section. (e) Cross sectional brightfield image of the scattering end of the fiber in (d).

2.3 Measuring scattering coefficient dependence on temperature and time

To measure the intrinsic optical loss of the fibers, we used a cutback technique. The measured loss of an 800 µm-thick PES fiber was 0.7 to 0.8 dB/cm at 633 nm, which corresponds to an attenuation coefficient α_0 of 0.16 to 0.18 cm^{-1}. This value was consistent with the optical loss of the bulk polymer in Fig. 1(a), which indicates that the surface roughness of the PES fiber prior to heat treatment is negligible compared to the material loss.

Next, we cleaved fibers with two different diameters, 300 and 800 µm, into shorter segments 20-30 mm-long, and applied heat along the entire lengths of the fibers using a hot flat-tip soldering iron. The amount of scattering increases with increasing heat exposure time as shown in Fig. 3(a). Note the heat treatment involves some axial shrinkage of the fibers due to release of the tension which was stored in the fiber during the draw [22]. The two ends of each fiber sample were then cut and polished, and the optical propagation loss of each fiber at 633 nm was measured as depicted in Fig. 3(b). From the data, we obtained the total attenuation coefficient, $\alpha = [ln(\text{loss})]$ cm^{-1}, of the fiber, and determined the coefficient of microbubble-induced scattering from the difference in optical loss, $\alpha - \alpha_0$, where α_0 is the attenuation coefficient of fiber prior to heat treatment. In Fig. 3(c), the fiber samples were heated for the same amount of time (6 s for 800 µm-diameter fibers and 5 s for 300 µm-diameter fibers), but at different temperatures (ranging from 140 to 200 °C) that were

Optics EXPRESS

measured using a thermocouple in contact with the fibers. In the second test, Fig. 3(d), the fiber temperature was maintained at 200 °C as the exposure time increased from 1 to 5 s for the 300 µm-diameter fibers and from 3 to 8 s for 800 µm-diameter fibers. We did not observe any change in the thicker fiber before 3 seconds. The results show that the scattering coefficient can be tuned by varying temperature and exposure time.

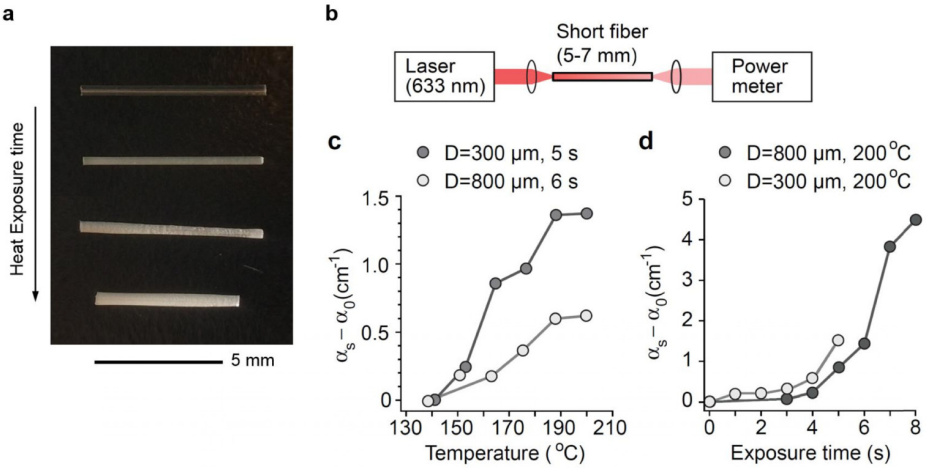

Fig. 3. Controlling the optical scattering of PES fibers. (a) Photograph of four PES fibers with different scattering coefficients. The top fiber is intact while the rest have been heated for different amounts of time. (b) A schematic of the experimental setup for measuring the optical scattering of the PES fibers. Measured scattering coefficients of different fibers (subtracted from the optical loss of an intact fiber of the same length, α_0) prepared at different temperatures, (c), and with exposure times, (d). The original fiber outer diameters (D) are 800 and 300 µm, respectively. The experimental error for (c) and (d) is less than 0.2 cm^{-1}.

2.4 Tunable scattering coefficients and designer emission patterns

To gain deeper insights into the formation of microbubbles, we fabricated an 800 µm-diameter fiber and treated a 5 mm-long distal section with an axially-varied heat exposure profile, increasing heating time toward the end of the section shown in Fig. 4(a). The axially increasing α_s resulted in a relatively uniform side emission profile shown in Fig. 4(b). To examine the microbubbles along the length, we cleaved the fiber into several 300 µm-thick segments. Figure 4(c) shows the cross-sectional transmission images of the segments. We found that the bubbles formed predominantly ~30 µm inside from the outer surface (sections 2 to 5). We reasoned that the moisture in the region closer to the surface managed to diffuse out of the fiber as temperature increased, preventing microbubbles from being formed. The diameter of the average microbubble is several microns wide.

The tunability of scattering was harnessed to achieve user-defined side-emission patterns. Figure 5(a) shows a 200 µm-thick fiber that was heat-treated to have a 1 cm-long uniform side-emission region according to a user-defined scattering profile, displayed in Fig. 5(b). We mounted the fiber on a 360-degree rotational stage and captured the emission profile as a function of the azimuthal angle. The result in Fig. 5(c) shows uniform angular scattering in all directions. Figure 5(d) depicts the normalized emission profile (magenta curve) in comparison to theoretical prediction (black curve) based on the target design profile. For further comparison, in Fig. 5(d) we also show the normalized emission profiles of two other fibers with the same outer diameter (200 µm) heat-treated with constant scattering coefficients of α_s = 0.25 mm^{-1} (dark green curve) and 2.5 mm^{-1} (light green curve), respectively. For the high-scattering fiber, light emission is localized in the first 1 mm length of the treated zone. For the low-scattering fiber, light emission intensity decreases exponentially with distance. The

Optics EXPRESS

increased brightness near the fiber end is due to the back scattering of remaining light at the end surface.

In another PES fiber, we introduced four scattering spots by applying local heat at discrete locations using a soldering iron tip, shown in Fig. 6(a). The scattering coefficient was increased by changing the exposure time such that an equal emission intensity was achieved from the four spots when light enters from the left, shown in Fig. 6(b).

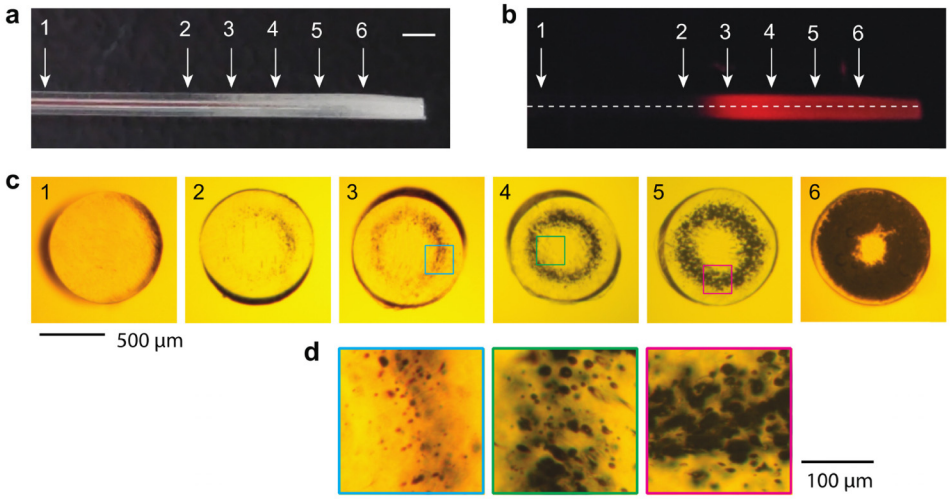

Fig. 4. (a) Photograph of an 800 µm-thick PES fiber in which the α_s varies axially (scale bar = 1 mm). (b) Side emission of the same PES fiber with red light entering from the left facet. (c) Brightfield cross-sectional images of various 300 µm-thick slices obtained from the fiber. Dark spots correspond to microbubbles. (d) Magnified images of the square regions marked in slices 3, 4, and 5 in (c).

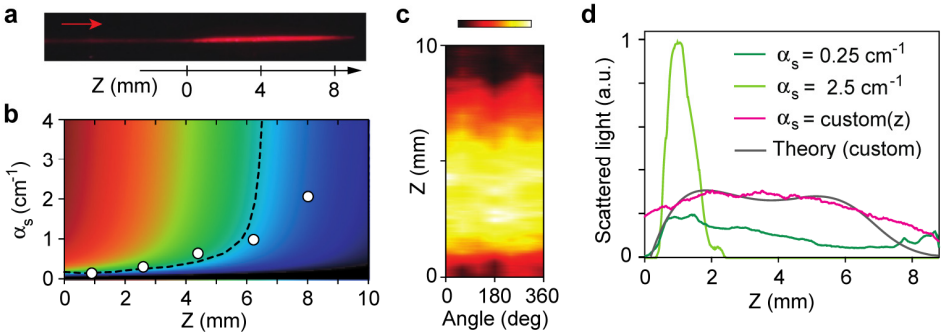

Fig. 5. (a) Side emission of a 200 µm-thick PES fiber. (b) User-designed scattering coefficient profile. Dotted line, an ideal curve for uniform side-emission or design target. Circles, the actual design target. The background colors show the target α_s values for specific fiber lengths (red, 0 mm, to blue, 10 mm). (c) Radial emission profile of the fiber. (d) The side emission profiles of the fiber with the custom scattering profile (magenta line: experiment; black line: theoretical prediction) and two fibers with different, constant scattering coefficients (light and dark green lines).

Optics EXPRESS

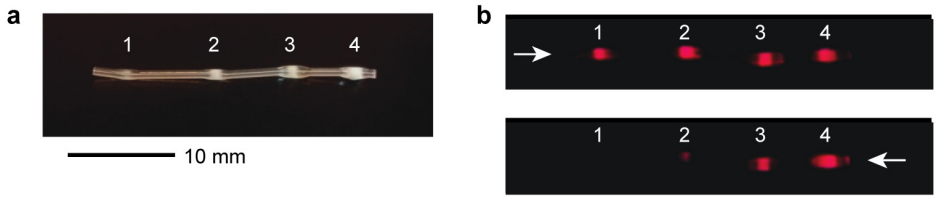

Fig. 6. A multiple-point emission fiber. (a) A photograph of a PES fiber with four scattering spots. (b) A side emission profile of the fiber for light entering from the left (top) or the right (bottom).

2.5 Surface-induced microbubbles for side light collection

Direct contact with a hot wire offers another way to generate micro-scatterers on PES fibers, as shown in Fig. 7(a). This technique is effective to introduce a localized side scattering spot, which may be used to emit light to a specific direction or, conversely, receive light from the side into the fiber. Incident light from the side is first scattered into various angles, and part of the forward scattered light may be captured into the fiber by total internal reflection at the opposite surface. The collection efficiency may be enhanced by introducing a second side scattering spot on the opposite fiber side as shown in Fig. 7(b). To make the scattering spot, we used a heating wire at a temperature of 450 °C and made contact to a PES fiber for a fraction of second. Figure 7(c) shows micrographs of a scattering spot made on an 800 μm-diameter fiber. Figure 7(d) shows a sample with a single scattering spot. When collimated, laser light (633 nm) was illuminated normal to the scattering spot, we measured 11% of the input light coupled into the fiber (by measuring the power at the fiber ends and considering the material and Fresnel losses). We then introduced the second scattering spot at the opposite surface, as shown in Fig. 7(e). The size of the second scattering spot was approximately made to be 1.2 mm wide ($2D*\tan\theta_c$ where D is the fiber diameter and θ_c = 37.3° is the critical angle for $n_{(PES)}$ = 1.65 and $n_{(air)}$ = 1). This resulted in a light collection efficiency increase from 11 to 19%.

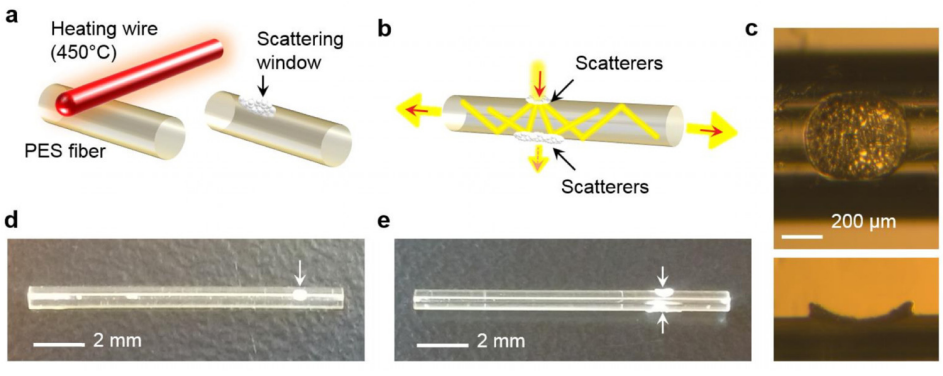

Fig. 7. (a) Schematic showing the formation of highly scattering surface spots on the PES fiber side. (b) Illustration demonstrating the use of dual scattering spots for light collection. (c) Close-up view of the scattering spot; front and side. (d) A photograph of a fiber with one scattering spot. (e) A photograph of a PES fiber with two scattering spots.

3. Conclusions

The intrinsic optical loss of 0.2 - 0.8 dB/cm of the PES fibers in the red and near infrared spectral ranges make them unsuitable for optical transmission across long distances. Indeed,

Optics EXPRESS

the simple post-processing techniques we introduced here render PES fibers as an attractive platform to fabricate short fiber segments (~cm's), with user-designable, side-illumination patterns. Short PES fibers with radially uniform illumination patterns can be connected to conventional low-loss optical fibers for practical applications such as photodynamic therapy or phototherapy in a hollow organ. The light-collection capability via side-scattering windows may then be useful for optical sensing and therapy monitoring. In this work, we utilized a soldering iron for heating, but the resolution and precision of the thermal post-processing could be further improved by making use of tightly focused laser heating.

Funding

U.S. Air Force Office of Scientific Research (AFOSR; FA9550-17-1-0277), National Institutes of Health (NIH; R01CA192878, P41 EB015903), and the Korea Institute of Science and Technology (KIST ORP Program, 2E27830, 2E27833).

References

1. S. Shabahang, S. Kim, and S. Yun, "Light-Guiding Biomaterials for Biomedical Applications," Adv. Funct. Mater. **28**(24), 1706635 (2018).
2. T. Hirano, Y. Hashimoto, H. Tanaka, I. Yamada, and K. Hashimoto, "Interstitial photodynamic therapy with moving exposure fiber," Methods Mol. Biol. **196**, 331–341 (2002).
3. H. Tanaka, K. Hashimoto, I. Yamada, K. Masumoto, T. Ohsawa, M. Murai, and T. Hirano, "Interstitial photodynamic therapy with rotating and reciprocating optical fibers," in *20th Congress of the Japan Society for Laser Surgery and Medicine* (American Cancer Society, 2001), **91**(9), pp. 1791–1796.
4. M. A. Kosoglu, R. L. Hood, J. H. Rossmeisl, Jr., D. C. Grant, Y. Xu, J. L. Robertson, M. N. Rylander, and C. G. Rylander, "Fiberoptic microneedles: Novel optical diffusers for interstitial delivery of therapeutic light," Lasers Surg. Med. **43**(9), 914–920 (2011).
5. M. A. Kosoglu, R. L. Hood, and C. G. Rylander, "Mechanical strengthening of fiberoptic microneedles using an elastomeric support," Lasers Surg. Med. **44**(5), 421–428 (2012).
6. V. G. Truong, S. Park, V. N. Tran, and H. W. Kang, "Spatial effect of conical angle on optical-thermal distribution for circumferential photocoagulation," Biomed. Opt. Express **8**(12), 5663–5674 (2017).
7. S. Nizamoglu, M. C. Gather, M. Humar, M. Choi, S. Kim, K. S. Kim, S. K. Hahn, G. Scarcelli, M. Randolph, R. W. Redmond, and S. H. Yun, "Bioabsorbable polymer optical waveguides for deep-tissue photomedicine," Nat. Commun. **7**(1), 10374 (2016).
8. P. M. Ripley, A. J. MacRobert, T. N. Mills, and S. G. Bown, "A Comparative optical analysis of cylindrical diffuser fibres for laser therapy using fluorescence imaging," Lasers Med. Sci. **14**(4), 257–268 (1999).
9. L. M. Vesselov, W. Whittington, and L. Lilge, "Performance evaluation of cylindrical fiber optic light diffusers for biomedical applications," Lasers Surg. Med. **34**(4), 348–351 (2004).
10. S. I. Park, D. S. Brenner, G. Shin, C. D. Morgan, B. A. Copits, H. U. Chung, M. Y. Pullen, K. N. Noh, S. Davidson, S. J. Oh, J. Yoon, K. I. Jang, V. K. Samineni, M. Norman, J. G. Grajales-Reyes, S. K. Vogt, S. S. Sundaram, K. M. Wilson, J. S. Ha, R. Xu, T. Pan, T. I. Kim, Y. Huang, M. C. Montana, J. P. Golden, M. R. Bruchas, R. W. Gereau 4th, and J. A. Rogers, "Soft, stretchable, fully implantable miniaturized optoelectronic systems for wireless optogenetics," Nat. Biotechnol. **33**(12), 1280–1286 (2015).
11. L. Chaudet, M. Neil, P. Degenaar, K. Mehran, R. Berlinguer-Palmini, B. Corbet, P. Maaskant, D. Rogerson, P. Lanigan, E. Bamberg, and B. Roska, "Development of optics with micro-LED arrays for improved opto-electronic neural stimulation," in *Optogenetics: Optical Methods for Cellular Control* (SPIE Proc **8586**, 2013), 85860R.
12. D. R. Sparta, A. M. Stamatakis, J. L. Phillips, N. Hovelsø, R. van Zessen, and G. D. Stuber, "Construction of implantable optical fibers for long-term optogenetic manipulation of neural circuits," Nat. Protoc. **7**(1), 12–23 (2012).
13. L. Li, C. Liu, Y. Su, J. Bai, J. Wu, Y. Han, Y. Hou, S. Qi, Y. Zhao, H. Ding, Y. Yan, L. Yin, P. Wang, Y. Luo, and X. Sheng, "Heterogeneous integration of microscale GaN light-emitting diodes and their electrical, optical, and thermal characteristics on flexible substrates," Adv. Mater. Technol. **3**(1), 1700239 (2018).
14. M. Irfan and A. Idris, "Overview of PES biocompatible/hemodialysis membranes: PES-blood interactions and modification techniques," Mater. Sci. Eng. C **56**, 574–592 (2015).
15. G. Tao, S. Shabahang, E. H. Banaei, J. J. Kaufman, and A. F. Abouraddy, "Multimaterial preform coextrusion for robust chalcogenide optical fibers and tapers," Opt. Lett. **37**(13), 2751–2753 (2012).
16. S. Shabahang, G. Tao, M. P. Marquez, H. Hu, T. R. Ensley, P. J. Delfyett, and A. F. Abouraddy, "Nonlinear characterization of robust multimaterial chalcogenide nanotapers for infrared supercontinuum generation," J. Opt. Soc. Am. B **31**(3), 450–457 (2014).
17. B. Temelkuran, S. D. Hart, G. Benoit, J. D. Joannopoulos, and Y. Fink, "Wavelength-scalable hollow optical fibres with large photonic bandgaps for CO2 laser transmission," Nature **420**(6916), 650–653 (2002).
18. S. Shabahang, G. Tao, J. J. Kaufman, Y. Qiao, L. Wei, T. Bouchenot, A. P. Gordon, Y. Fink, Y. Bai, R. S. Hoy,

Optics EXPRESS

and A. F. Abouraddy, "Controlled fragmentation of multimaterial fibres and films via polymer cold-drawing," Nature **534**(7608), 529–533 (2016).
19. G. Baschek, G. Hartwig, and F. Zahradnik, "Effect of water absorption in polymers at low and high temperatures," Polymer (Guildf.) **40**(12), 3433–3441 (1999).
20. S. Velu, L. Muruganandam, and G. Arthanareeswaran, "Preparation and performance studies on polyethersulfone ultrafiltration membranes modified with gelatin for treatment of tannery and distillery wastewater," Braz. J. Chem. Eng. **32**(1), 179–189 (2015).
21. AZoM, *Polyethersulphone (PES) - Supplier Data* (2003).
22. S. Shabahang, G. Tao, J. J. Kaufman, and A. F. Abouraddy, "Dispersion characterization of chalcogenide bulk glass, composite fibers, and robust nanotapers," J. Opt. Soc. Am. B **30**(9), 2498–2506 (2013).